



Parameter Sensitivity Study on Static and Dynamic Mechanical Properties of the Spatial Y-shaped Tied Arch Bridge

Jianpeng Sun^{1,2} · Zihan Tan^{1,2} · Jiaju Zhang^{1,2} · Wenwu Sun^{1,2} · Li Zhu³

Received: 26 April 2022 / Accepted: 7 December 2022 / Published online: 20 December 2022
© Korean Society of Steel Construction 2022

Abstract

The spatial Y-shaped tied arch bridge is a rare form of innovative bridge on arch bridges around the world. It has important reference significance for the design and construction of bridge engineering worldwide. This arch bridge is novel in design and adopts single and double arch ribs combined structure. However, as a novel bridge type, its force situation is indetermination, so it is very important to study its mechanical properties and parameter sensitivity. In order to study the mechanical properties of the spatial Y-shaped tied arch bridge and the influence of structural parameters, this paper takes a spatial Y-shaped tied arch bridge under construction in China as the research object. The finite element software MIDAS Civil is used to establish the bridge model. The finite element model is used to analyze the static and dynamic performance of the spatial Y-shaped tied arch bridge under the use stage and the mechanical change trend under the influence of different rise-span ratios and double arch bifurcation angles. The results of single arch rib and double arch rib under constant load and live load are compared under different structural parameters in this paper, and the parameter sensitivity analysis of statics and dynamics is carried out. These analyses provide the adjustment basis and design reference for the design of the special-shaped arch bridge in the future.

Keywords Special-shape arch bridge · Mechanical property · Static analysis · Dynamic analysis · Structural parameter analysis · Parameter Sensitivity

1 Introduction

With the extensive use of steel in bridge engineering, the construction of steel arch bridges is increasing (Feng et al., 2021; Kasimzade et al., 2021; Sui et al., 2020; Sun & Tan, 2022; Sun & Zhufu, 2022; Sun et al., 2020, 2021, 2022a, b, c, d; Tabar et al., 2021). Compared with the ordinary reinforced concrete arch bridge and the concrete-filled steel tube arch bridge, the steel arch bridge is more convenient and quicker to construct and has the characteristics of small weight, small horizontal thrust, and large span (Backer et al., 2014; Jin and Li, 2009; Liu et al., 2014b; Lonetti et al., 2018). The construction of steel arch bridges in China started late, but with the rapid development of China's economy and infrastructure in recent years, the construction of steel arch bridges has also been a great development (Zhou & Zhang, 2019). At the same time, the development of construction technology and structural form has enabled bridge designers to gradually add fantastic ideas to the bridge and realize them, making the traditional arch bridge gradually develop a series of new special-shaped bridges, such as inclined arch

✉ Zihan Tan
tanzihanyx@163.com

Jianpeng Sun
sunjianpeng2001@163.com

Jiaju Zhang
770876645@qq.com

Wenwu Sun
615713513@qq.com

Li Zhu
59348804@qq.com

¹ School of Civil Engineering, Xi'an University of Architecture and Technology, Xi'an 710055, Shaanxi, China

² Institute for Interdisciplinary and Innovate Research, Xi'an University of Architecture and Technology, Xi'an 710055, Shaanxi, China

³ Xi'an Jianzhukeda Engineering Technology Co., Ltd, Xi'an 710055, Shaanxi, China

bridges, butterfly arch bridges, inclined span arch bridges, arch tower cable-stayed bridges and so on (Huo & Han, 2014; Kou et al., 2011; Li et al., 2004; Lu et al., 2009; Wang et al., 2011). These new arch bridge types not only have the round and dynamic aesthetic characteristics of traditional arch bridges but also constantly refresh the limits of people's aesthetic imagination of bridges. For example, the Bacde Road Bridge (Liu et al., 2014a), the Gateshead Millennium Bridge (White & Fortune, 2012), and the JK Bridge (Batista & Ghavami, 2005) are among the masterpieces of these new special-shaped arch bridges. Although the construction of special-shaped arch bridges in China started late, there are still many excellent projects known around the world, such as the Wuchazi Bridge (Ye, 2020), the Jiulong River Bridge (Liu et al., 2015), the Shizhi River Bridge (Lu et al., 2021) and other special-shaped arch bridges. Compared with the traditional arch bridge, the special-shaped arch bridge has the advantages of a unique appearance and easy combination with the environment around the bridge site. The built special-shaped arch bridge shows that most of the special-shaped arch bridges have become locally famous scenic spots. The special-shaped steel arch bridge has become a new development trend of steel arch bridges.

Although the special-shaped arch bridge has the aesthetic characteristics of novel design and unique structure, it also has the disadvantages of complex structure, difficult construction, and high maintenance cost. Therefore, the construction of the special-shaped arch bridge needs to analyze the static and dynamic mechanics and the sensitivity of design parameters. In recent years, more and more researchers focus on the static and dynamic characteristics of special-shaped arch bridge design. Cheng used ANSYS to analyze the static and dynamic characteristics of the Yingzhou Bridge and studied the mechanical behavior of this bridge in extreme events, which provided a reference for the design of special-shaped arch bridges with similar structures in the future (Cheng et al., 2017). Wu established a fine three-dimensional finite element model of a butterfly-shaped arch bridge to analyze the static and dynamic characteristics and compared it with the numerical analysis and field tests, and corrected the finite element model. The updated model thus obtained can be treated as a baseline finite element model, which is suitable for long-term monitoring and safety evaluation of the structure (Wu et al., 2021). Design parameters are the influencing factors that can adjust or even determine the mechanical properties of bridges in bridge design, the analysis of structural parameter sensitivity has always been the focus of structural design (Cheng et al., 2021; Svendsen et al., 2021; Wang et al., 2014). The parameter sensitivity analysis of the special-shaped arch bridge with a new structure is helpful for scholars to understand the mechanical properties of the new structure better, and it can also provide

a reference for the design of similar special-shaped arch bridges in the future. In recent years, many researchers have begun to analyze the parameter sensitivity of special-shaped arch bridges (Banerji and Chikermane, 2012; Li et al., 2018, 2020; Qin et al., 2022; Shi et al., 2020; Tubaldi et al., 2019; Zhang et al., 2020). These studies studied the influence of different parameters on the static and dynamic characteristics of the bridge and provided a solid theoretical guarantee for the design and development of the special-shaped arch bridge.

The half-through tied arch bridge is a kind of bridge type that combines the advantages of the arch and beam. It combines the two basic structural forms of arch and beam and gives full play to the structural performance and combination of beam and arch. It has the advantages of reasonable load, beautiful shape, simple structure, and easy construction. Therefore, its application in landscape bridges is increasing gradually (Chen & Wang, 2009; He & Chen, 2014; Ma et al., 2021; Tang et al., 2014; Wu et al., 2018). In general, the main arch ribs of the half-through tied arch bridge are mostly bidirectional symmetrical, which makes the traditional half-through arch bridge have high requirements for the selection of bridge site and less arrangement form of the substructure. In the special terrain such as intersection terrain and tunnel entrance, the traditional half-through tied arch bridge has the disadvantages of affecting the driving sight and poor landscape performance (Fan et al., 2022; Li et al., 2018; Nonaka & Ali, 2001; Wu & Qiu, 2012).

In order to overcome the shortcomings of the traditional half-through tied arch bridge, the spatial Y-shaped tied arch bridge is designed in China. As a novel special-shaped arch bridge, the spatial Y-shaped tied arch bridge symmetry along bridge direction and adopts single and double arch ribs combined structure. This bridge can be flexibly arranged in special terrains such as canyons and river valleys. It has a good vision in the road crossing section and the tunnel portal section and has the advantages of good economic performance and excellent landscape performance. However, the spatial Y-shaped tied arch bridge is a rarely seen innovative practice around the world (Huang et al., 2022; Zhang, 2021), the unique bridge shape leads to its complex structure, and its mechanical properties are different from those of ordinary tied arch bridges. Its unique spatial Y-shaped arch rib makes the mechanical properties of this bridge fuzzier.

Therefore, this paper takes a spatial Y-shaped tied arch bridge under construction as the object to study the static and dynamic mechanical properties of the spatial Y-shaped tied arch bridge and their parameter sensitivity, which can guarantee the construction of the spatial Y-shaped tied arch bridge and provide a reference for the design and analysis of similar bridges in the future.

2 Engineering Example of the Spatial Y-shaped Tied Arch Bridge

The Jinghe Bridge is an essential node project in the external traffic engineering of Dongzhuang Water Conservancy Hub in Shaanxi Province, and it is an important scenic spot project in Guanzhong Canyon Tourism Belt. In order to pursue the landscape effect corresponding to the Dongzhuang Reservoir, the Jinghe Bridge integrates the structural characteristics of the butterfly arch bridge and half-through arch bridge in design. It not only has a beautiful bridge type and special shape but also adopts the combination form of separated main arch rib and secondary arch rib to form the spatial special-shaped structure, which further obtains better visual effect, the 3D model diagram of the spatial Y-shaped tied arch bridge is shown in Fig. 1.

As a novel large-scale landscape bridge, this bridge is a half-through spatial Y-shaped steel box arch bridge with a total length of 284 m. The calculated span of the main beam is $2 \times 19.5m + 197m(14.5m + 28 \times 6m + 14.5m) + 2 \times 19.5m$. The arch bridge is mainly composed of main arch rib, secondary arch rib, arch footing, main-secondary arch connecting rib, suspender, main beam, and other components. The main arch rib is a catenary variable cross-section box arch with a horizontal projection of Y-shape, which is mainly composed of single arch rib and double arch rib. The main arch is an arch without hinge points. The side span and main span of the main beam are both suspended continuous beam structures. The clear span of the main span is 220 m, the arch rise is 62.5 m, and the rise-span ratio is 1/3.52. The layout of the half-through spatial Y-shaped tied arch bridge is shown in Fig. 2.

This bridge adopts the second-class highway technical standard, the design speed is 40 km/h, and the

two-way two-lane is arranged in the transverse direction of the bridge. The standard cross-section layout is: sidewalk(2.75 m) + side strip(0.25 m) + motored-vehicle lane(3.75 m) + side strip(0.25 m) + medial strip(4 m) + side strip(0.25 m) + motored-vehicle lane(3.75 m) + side strip(0.25 m) + sidewalk(2.75 m), a total of 18 m, The diagram of the main beam standard cross-section is shown in Fig. 3.

2.1 Main Arch Rib

The main arch rib is a spatial Y-shaped variable cross-section box arch. The catenary arch has the characteristics of less material and light weight, modern construction technology and materials can guarantee its strength and accuracy. Therefore, modern bridges generally use a catenary as the most ideal arch axis (Zhang et al., 2019). So in the design of the spatial Y-shaped tied arch bridge, the facade projection of the arch axis is catenary, whose equation is:

$$y = f \times (\cosh k\xi - 1)/(m - 1) \quad (1)$$

$$k = \ln(m + \sqrt{m^2 - 1}) \quad (2)$$

$$\xi = \frac{x}{l} \quad (3)$$

where, f is the height of the arch axis, that is, the vertical height from the arch footing to the arch vault; l is the length of the arch axis, that is, the horizontal distance from the arch footing to the arch vault; m is the arch axis coefficient; x and y are the independent and dependent variables of catenary equation respectively.

For this bridge, the clear span is 220 m (corresponding to pile number: K35 + 205.000 to K35 + 425.000), the clear



Fig. 1 3Dmodel diagram of the spatial Y-shaped tied arch bridge

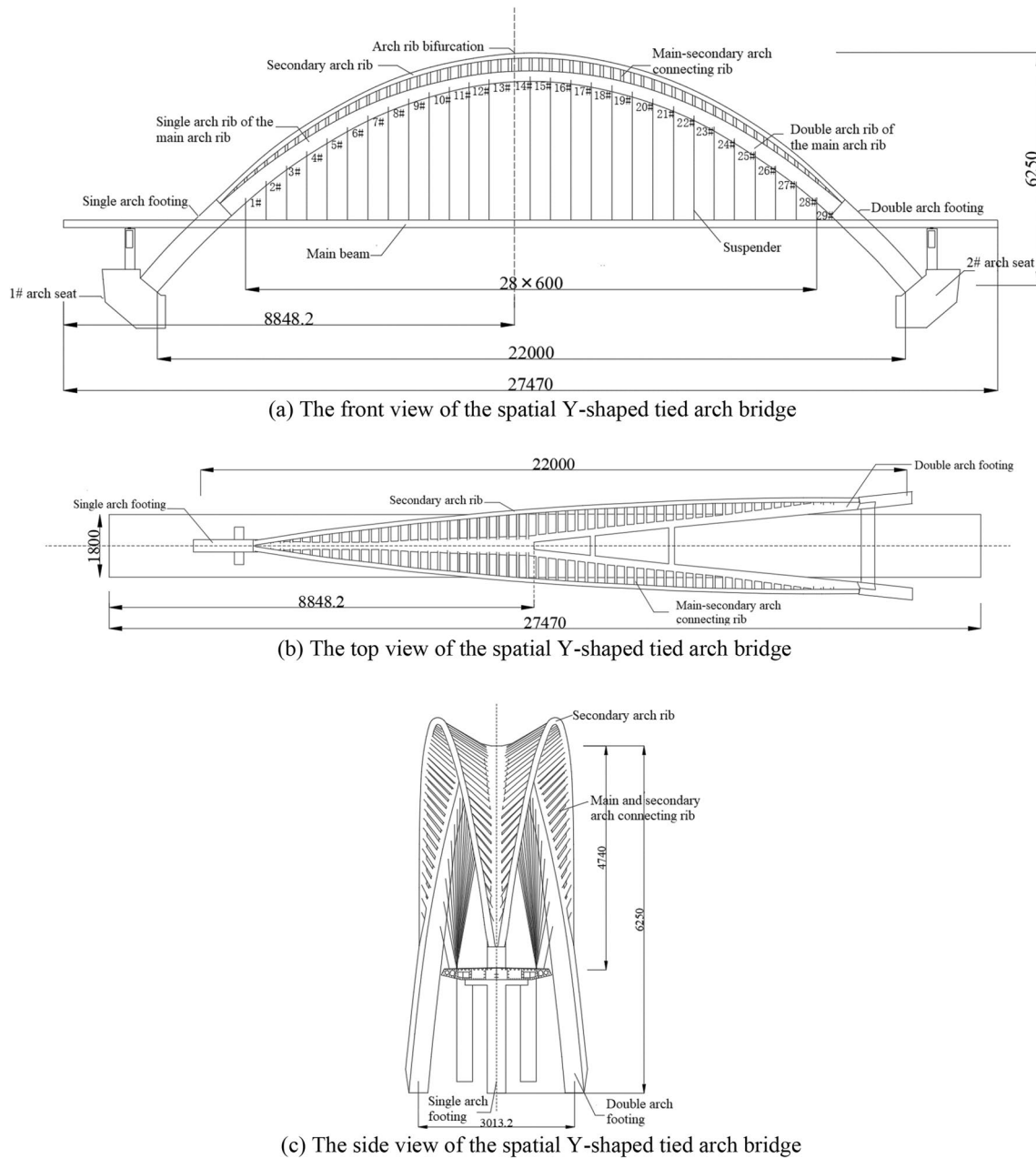


Fig. 2 The layout diagram of the spatial Y-shaped tied arch bridge (unit: cm)

arch rise is 62.5 m, the arch axis coefficient $m = 1.347$, and the rise-span ratio is 1/3.52. The horizontal projection of the arch axis is Y-shape. The single arch rib is arranged on the right side of the Jing River, and the double arch rib is arranged on the left side of the Jing River. The axis is bifurcated from K35 + 288.500, and the bifurcation angle is 12.42°.

The sectional dimension of the single arch rib gradually changed from 3.5 m × 6.6 m to 3.293 m × 3.558 m from the arch footing to the arch vault, and the sectional dimension of the double arch rib gradually changed from 3.5 m × 6.6 m

to 2.023 m × 3.075 m from the arch footing to the arch vault. The main arch rib is divided into 17 segments along the bridge direction. The segment numbers are ZS0 to ZS16 respectively, and the maximum weight of a single stage is 130.7t.

2.2 Partial Design of the Main Arch Rib

Wind brace: The whole bridge is provided with two one-line wind braces between the double arch ribs. Both of the wind braces adopt the rectangular steel box section, the thickness

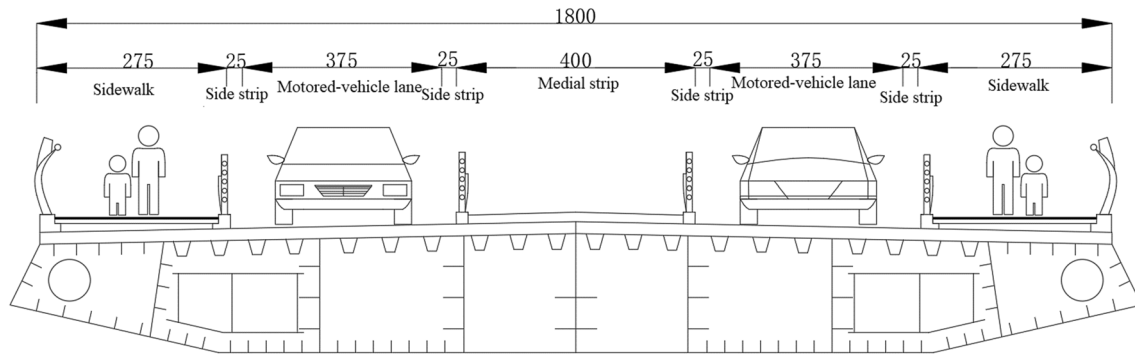


Fig. 3 The diagram of the main beam standard cross-section (unit: cm)

is 20 mm, the width is 1.5 m, and the height is equal to the arch rib height.

Cross beam: A cross beam is set at the intersection of arch ribs and main beams on both sides of the bridge. The main beam is supported by bridge bearings. The cross beam of the single arch rib adopts a variable height rectangular steel box section, the section size is $4.0\text{ m} \times (3.5\text{ m} \sim 2.5\text{ m})$. The cross beam of the double arch rib adopts an equal height rectangular steel box section, the section size is $4.0\text{ m} \times 3.5\text{ m}$.

2.3 Secondary Arch Rib and Main-Secondary Arch Connecting Rib

The secondary arch rib is a spatial three-dimensional structure, and it is symmetrically arranged on both sides of the main arch rib by a 5° outward inclination of the connection around the starting and ending points of its own axis. The arch axis is catenary, whose equation is Eq. (1). The clear span of the secondary arch rib is 184.5 m, the clear arch rise is 43 m, the rise-span ratio is $1/4.29$, and the arch axis coefficient is 1.756.

The secondary arch rib adopts a circular steel tube section with a diameter of 1.4 m and a thickness of 24 mm; the stiffening rib is the plate rib with a thickness of 12 mm; The thickness of the transverse diaphragm is 12 mm, and the transverse diaphragm is arranged to correspond to the side

web of the main-secondary arch connecting rib. The main arch rib and the secondary arch rib are connected by the main-secondary arch connecting rib. The axis of the main-secondary arch connecting rib is a circular curve, which changes step by step from the arch footing to the arch vault. The main-secondary arch connecting rib adopts the box section, whose size is $0.7 \times 1.0\text{ m}$, and the thickness is 20 mm.

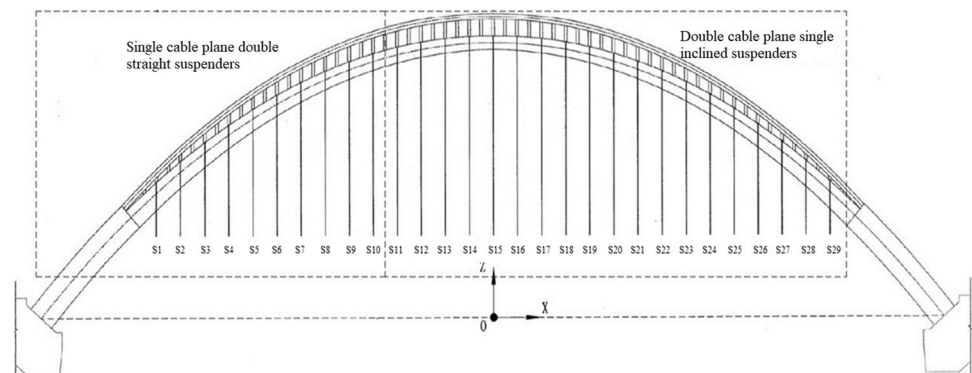
2.4 Suspender

There are 29 pairs of suspenders in the spatial Y-shaped tied arch bridge, and the standard spacing between the suspenders is 6 m. The single cable plane double straight suspenders S1~S10 are set at the single arch rib. The double cable plane single inclined suspenders S11~S29 are set at the double arch rib. The suspenders adopt three kinds of epoxy sprayed steel wire finished rope (PES.E7-55, PES.E7-61, and PES.E7-73) and supporting anchorage. The suspender number is shown in Fig. 4.

2.5 Main Beam

The main beam of the bridge is a Π -shaped double-box and double-chamber steel box beam. The main beam length is 274.7 m and the standard cross-section width is 18.0 m. The main beam is divided into 36 segments,

Fig. 4 Suspender numbers



the segment number is LS0~LS35. The main beam is divided into three kinds of cross-sectional forms: (a) The single cable plane double suspender cross-section; (b) The double cable plane single suspender cross-section; (c) The single arch rib separated cross-section. As shown in Fig. 5.

3 Establishment and Verification of the Finite Element Model

The finite element model of the whole bridge of the spatial Y-shaped tied arch bridge is established by MIDAS Civil. Because this paper is to analyze the mechanical properties and the structural parameter sensitivity of the bridge, the three-dimensional modeling method is used to calculate the

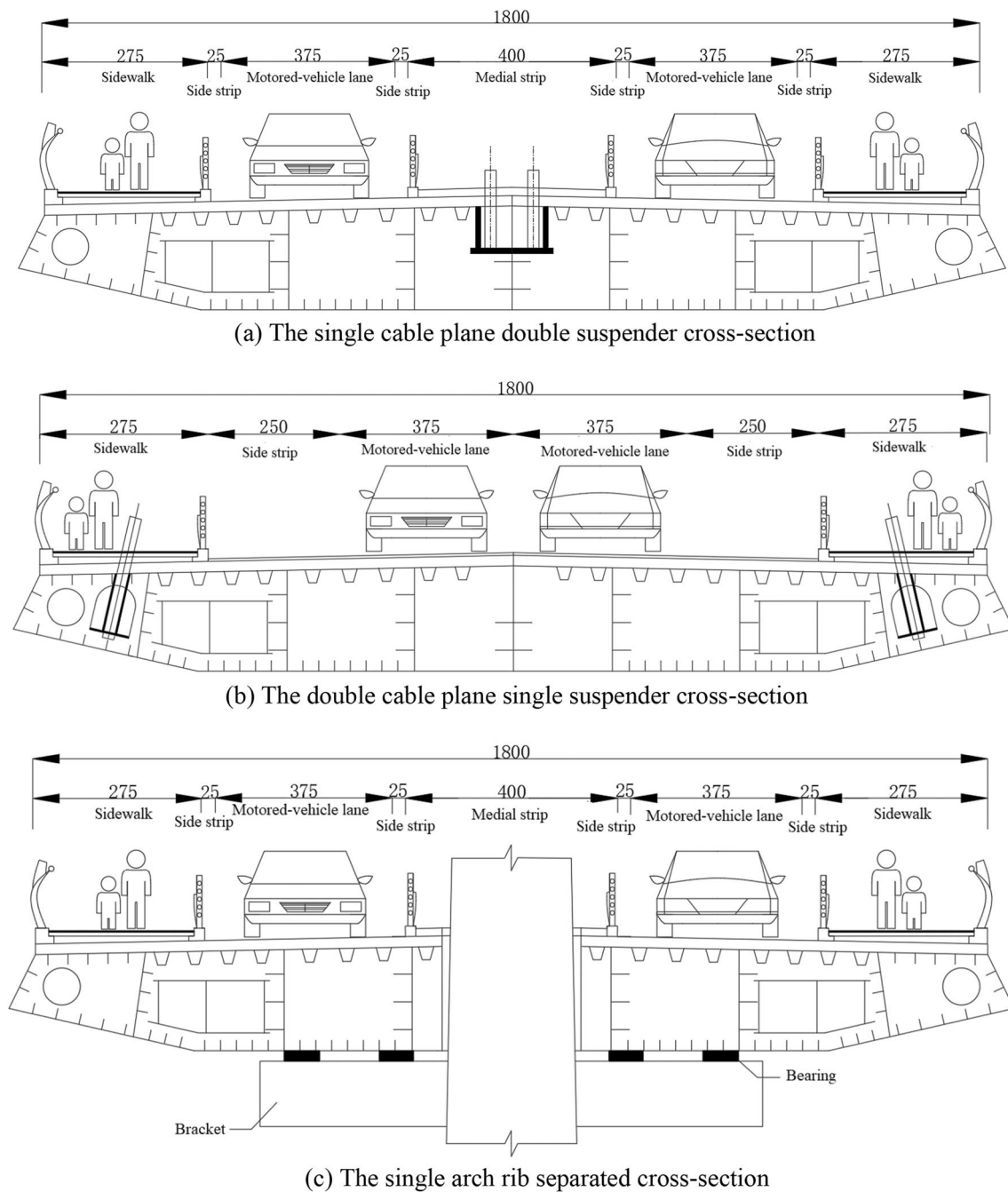


Fig. 5 Three kinds of cross-sectional forms of the main beam (unit:cm)

bridge at one time without considering the analysis of the construction stage. The finite element model of the bridge is established with an X-axis along the bridge and a Y-axis across the bridge. There are 889 joints and 968 elements (902 beam elements and 58 truss elements) in the finite element model. The main arch rib, secondary arch rib, main and secondary arch connection rib, and main beam are simulated by the beam element, and the suspenders are simulated by the truss element. The constant load and live load of the main beam are considered by the equivalent uniform load. The finite element model of the half-through spatial Y-shaped tied arch bridge is shown in Fig. 6. The main material properties of the model are shown in Table 1.

3.1 Simulation of the Main Arch Rib and Wind Brace

The main arch rib of the bridge is a special-shaped spatial structure composed of two arch ribs, which are the single arch rib and the double arch rib respectively. The double arch rib is symmetrical along the middle line of the single arch rib. The main arch rib of the half-through spatial Y-shaped arch bridge consists of 17 segment types. Because the main arch rib adopts the structural form without hinge

points, the connection between the main arch rib and the secondary arch rib and the bifurcation of arch ribs are simply simulated respectively. The connection of the main arch rib and the secondary arch rib and the bifurcation of arch ribs are consolidated by rigid connection. This bridge is equipped with two wind braces, both of which are simulated by a box-shaped equal section beam element. The finite element model of the main arch rib and the wind brace is shown in Fig. 7.

3.2 Simulation of the Secondary Arch Rib and the Main-Secondary Arch Connecting Rib

According to the bridge design data, the secondary arch rib is a ribbed circular section, the main-secondary arch connection rib is a ribbed box section. In practical engineering, the axis of the main-secondary arch connection rib of the special-shaped arch bridge is a circular curve with the radius of curvature changing step by step with the distance between the main arch rib and the secondary arch rib. The main-secondary arch connecting ribs are the non-important load-bearing components of the spatial Y-shaped tied arch bridge. In this bridge, they mainly play the role of landscape

Fig. 6 The finite element model of the half-through spatial Y-shaped tied arch bridge

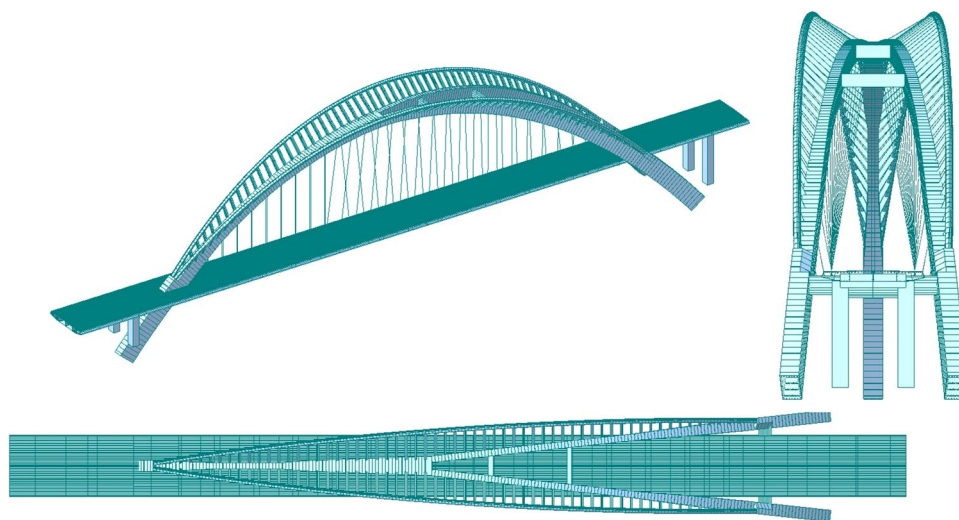
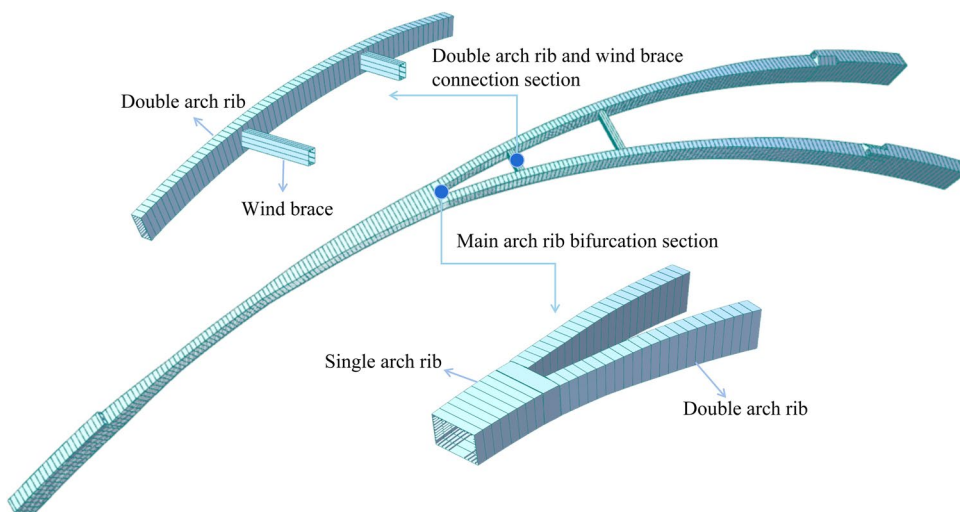


Table 1 The main material properties of the model

Material	Category	Component of the bridge	Material properties			
			Elastic modulus(MPa)	Poisson's ratio	Density (kN·m ⁻³)	Coefficient of linear expansion(1/°C)
Concrete	C50	Bridge piers Arch seats	3.15×10^4	0.2	25	1.0×10^{-5}
Steel strand	Strand1860	Suspenders	2.05×10^5	0.3	76.98	1.2×10^{-5}
Steel	Q420qDNH	Arch ribs main beam	2.06×10^5	0.3	76.98	1.2×10^{-5}

Arch ribs include the main arch rib, secondary arch rib, main-secondary arch connecting rib, wind brace, and cross beam

Fig. 7 The finite element model of the main arch rib and the wind brace



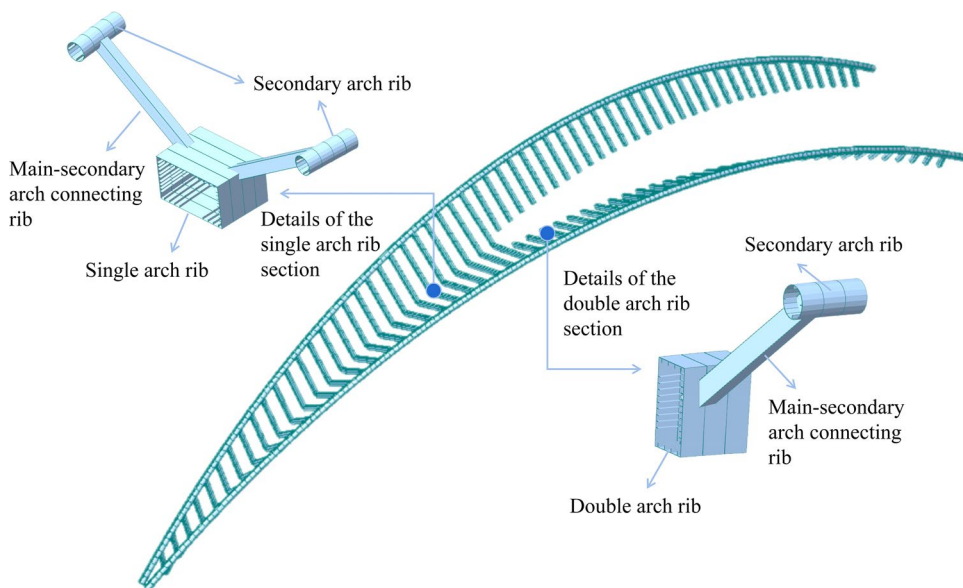
and the connection between the main arch rib and the secondary arch rib. Therefore, in order to ease the establishment of the model, the axis of the main-secondary arch rib is simplified from a circular curve to a straight line in the establishment of the finite element model, and the missing mass is converted into a uniform load applied to the connection rib. The finite element model of the secondary arch rib and the main-secondary arch connection rib is shown in Fig. 8.

3.3 Simulation of the Main Beam

The main beam of the spatial Y-shaped tied arch bridge is a II-shaped steel box beam with a horizontal projection length of 274.7 m. In the construction, it is divided into

36 segments for easy transportation and hoisting, and the segment numbers are LS0 ~ LS35 respectively. The cross-sections of segments from LS0 to LS33 are the standard cross-sections with a bridge width of 18 m. The LS34 and LS35 segments are the widening sections of the viewing platform. The bridge width is 36 m in these two segments. In the design of the bridge, the widening part of the LS34 and LS35 segments only considers the crowd load. In order to facilitate the establishment of the finite element model, the 34 and 35 segments are simplified. The widening section is simplified into a standard section, and the widening part is applied to both sides of the LS34 and LS35 standard sections in the form of load. The finite element model of the main beam is shown in Fig. 9.

Fig. 8 The finite element model of the secondary arch rib and the main-secondary arch connection rib



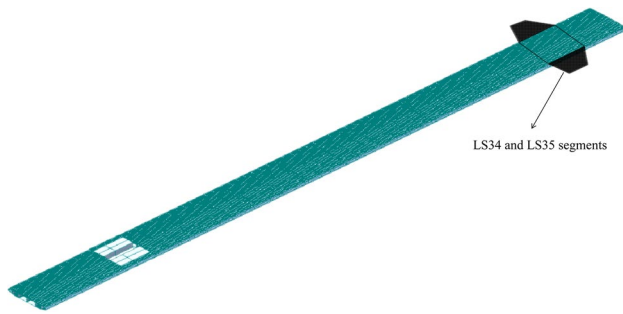


Fig. 9 The finite element model of the main beam

3.4 Boundary Conditions and Load Conditions

According to the design data, the half-through spatial Y-shaped arch bridge has two bridge bearings at bridge platforms, bridge piers, and cross beams respectively, and the whole bridge has 12 bridge bearings (the constraint points 1 ~ 12 in Fig. 10). The layout diagram of the constraint points is shown in Fig. 10, and the degree setting of freedom of the constraint points is shown in Table 2.

In addition to the constraints of bridge bearings, the simulation methods of other boundary conditions are as follows: (1) The connections between the suspenders and the main arch rib or the main beam adopt rigid connections; (2) The supports between the main beam and the brackets/ cross beams/ bridge piers/ bridge platforms adopt elastic connections; (3) The connections between the main-secondary arch connecting rib and the main arch rib

or the secondary arch rib adopt rigid connections; (4) The displacements and rotation constraints of the main arch rib (the constraint points 13 ~ 15 in Fig. 10) and the bottom of the bridge piers are carried out in three directions.

The load conditions of the spatial Y-shaped tied arch bridge are simulated as follows:

- (1) Gravity: The mass of the transverse diaphragm in the main arch rib, secondary arch rib, and main beam is converted into the node load input model, and the weight of other components in the finite element model is automatically calculated by MIDAS Civil;
- (2) The second constant load is 140kN/m;
- (3) The vehicle load grade is Highway-I, and the crowd load is $q = 2.5kN/m^2$ according to the General Specifications for Design of Highway Bridges and Culverts (JTG D60-2015).
- (4) Temperature: According to the full bridge heating 25 °C and cooling 25 °C to calculate.

3.5 Verification of the Finite Element Model

Combined with the relevant specifications (JTG, 2015; JTGT, 2015) of bridge design in China, in order to ensure that the finite element model can meet the structural design requirements, the load-carrying capacity and displacement of the finite element model should be verified, so as to ensure that the designed bridge can be used in practical engineering construction and provide reference for practical engineering construction.

Fig. 10 The layout diagram of the constraint points

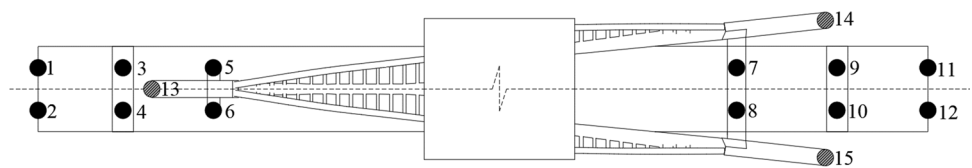


Table 2 the degree setting of freedom of the constraint points

Degree of freedom	1	2	3	4	5	6	7	8	9	10	11	12	13	14	15
X	1	1	0	0	0	0	0	0	0	0	0	0	1	1	1
Y	1	1	0	0	1	1	1	1	0	0	0	0	1	1	1
Z	1	1	1	1	1	1	1	1	1	1	1	1	1	1	1
R _x	0	0	0	0	0	0	0	0	0	0	0	0	1	1	1
R _y	0	0	0	0	0	0	0	0	0	0	0	0	1	1	1
R _z	0	0	0	0	0	0	0	0	0	0	0	0	1	1	1

X represents the longitudinal direction, Y represents the transverse direction, and Z represents the vertical direction

1 represents constraint, and 0 represents freedom

3.5.1 Verification of Load-Carrying Capacity

The verification of load-carrying capacity is mainly to verify whether the maximum stress of each component of the designed bridge is less than the allowable stress of the material. Since the suspender is simulated by the truss element and the rest of the steel components are simulated by the beam element, the combined stress of the beam element and the internal force of the truss element are checked respectively. According to the working condition: constant load + live load, the combination stress diagram of the beam element and the combined stress diagram of the truss element are shown in Figs. 11, 12.

The suspenders adopt Strand1860, whose yield strength is 1860 MPa, the maximum combined stress is 628.77 MPa from Fig. 12; and the rest of the steel components adopt Q420qDNH, whose yield strength is 420 MPa, the maximum combined stress is 156.13 MPa from Fig. 11.

Therefore, the load-carrying capacity of the established finite element model accords with the design requirements.

3.5.2 Verification of deformation

In accordance with Article 4.2.3 of *Specification for Design of Highway Steel bridge* (JTG, 2015) and Article 6.2.1 of *Specifications for Design of Highway Concrete-filled Steel Tubular Arch Bridges* (JTGT, 2015), the maximum vertical deformation of the arch rib is not over $L/1000$ (“L” denotes the span) and the vertical deformation of the main beam is not over $L/800$ under the action of moving load (vehicle load + crowd load). The vertical displacement of the arch rib and the vertical displacement of the main beam are shown in Figs. 13, 14 respectively.

From Fig. 13, it can be seen that the maximum vertical displacement of the arch rib under the moving load is 50.72 mm, the maximum vertical deformation of the arch rib is not over $L/1000$ (220 mm), which meets the design

Fig. 11 The combination stress diagram of the beam element (unit: MPa)

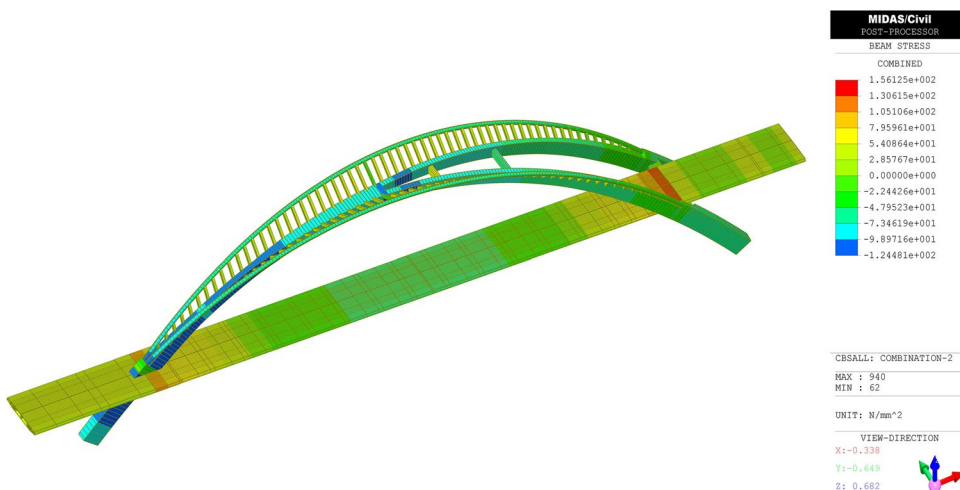


Fig. 12 The combination stress diagram of the truss element (unit: MPa)

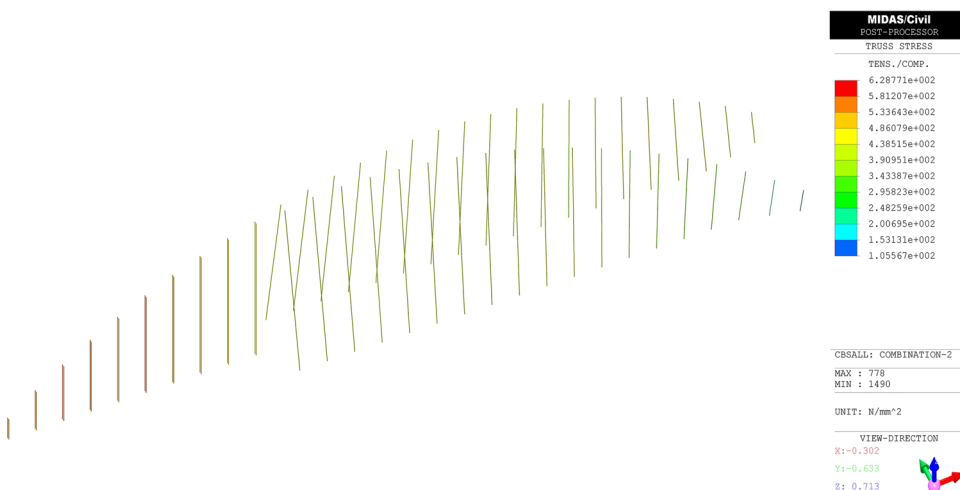


Fig. 13 The vertical displacement of the arch rib (unit: mm)

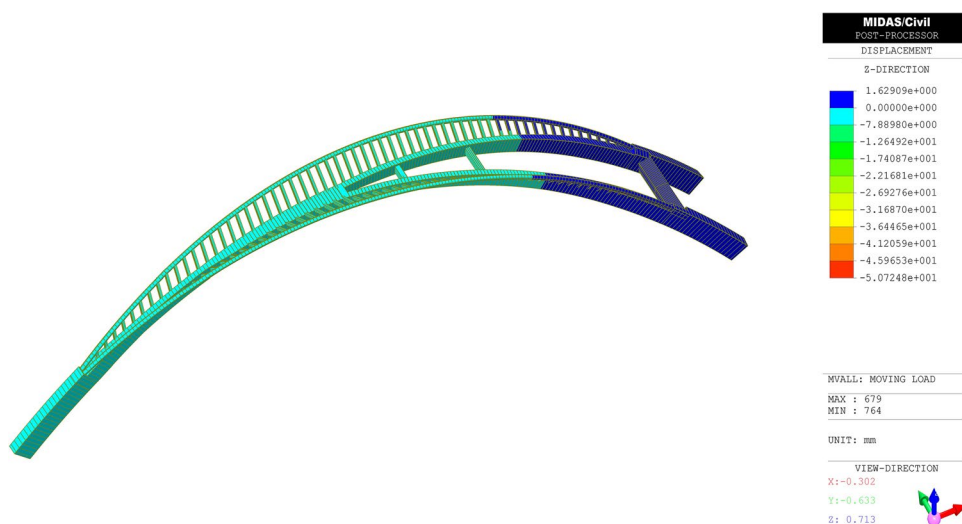
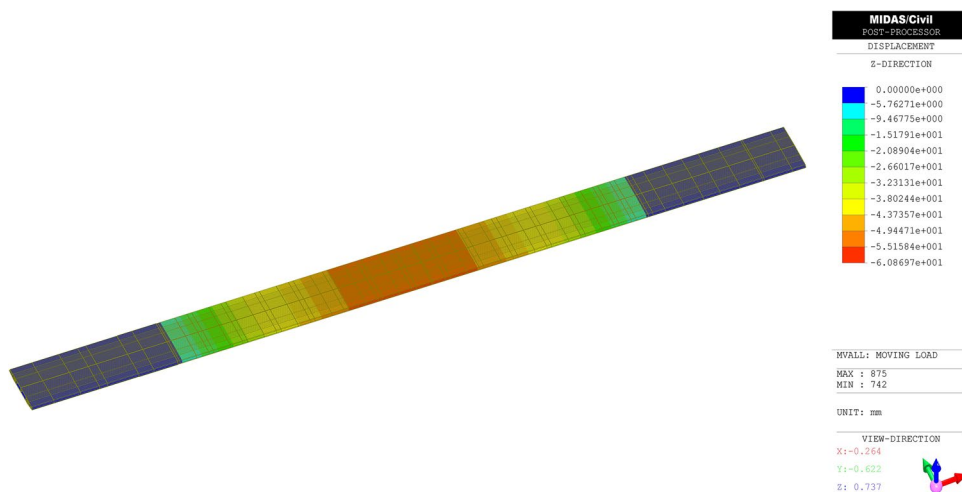


Fig. 14 The vertical displacement of the main beam (unit: mm)



requirement. From Fig. 14, it can be seen that the maximum vertical displacement of the main beam under the moving load is 60.09 mm, the maximum vertical deformation of the main beam is not over $L/800$ (275 mm), which meets the design requirement. Therefore, the deformation of the established finite element model accords with the design requirements.

In summary, the established finite element model meets the design requirements, and can provide reference for practical engineering construction.

4 Static Mechanical Properties and Parameter Sensitivity of the Spatial Y-shaped Tied Arch Bridge

4.1 Static Mechanical Properties of the Main Arch Rib

The main arch rib is one of the main load-bearing components of the spatial Y-shaped tied arch bridge, and its mechanical properties are very important to the design of the bridge. In order to study the static mechanical properties of the main arch rib under the use stage, the static analysis of the bridge will be carried out according to the following four working conditions (Zhu et al., 2022). Four working conditions are as follows: Working condition 1 is constant load; working condition 2 is constant load + live load; working condition 3 is constant

load + live load + full-bridge heating effect; working condition 4 is constant load + live load + full-bridge cooling effect. The displacement, bending moment, and axial force of the main arch rib under four working conditions are calculated. The results are shown in Fig. 15. Since the spatial Y-shaped tied arch bridge is symmetrical about the direction of the bridge, only the calculation results of the single arch rib and one side double arch rib are listed.

From the calculation results of Fig. 15, it can be seen that:

- (1) The deformation of the main arch rib in the use stage is sinusoidal under four working conditions, the double arch rib appears downward deflection deformation, and the single arch rib appears upward deflection deformation trend. The maximum displacement of the arch rib occurs at the double arch rib. By comparing the displacement under working condition 1 and working condition 2, it can be found that the displacement under live load exceeds 16% of the displacement under constant load, and the double arch rib is more sensitive to the live load. The temperature has a great influence on the double arch rib. The cooling full-bridge cooling effect has the greatest influence on the displacement of the main arch rib. The maximum displacement under the full-bridge heating effect is only 89.4 mm, and the maximum displacement under the full-bridge cooling effect can reach 268 mm.
- (2) The bending moment of the main arch rib is positively and negatively alternately distributed, and there are many turning points. The reason for this phenomenon may be that the main arch rib is affected by the secondary arch rib and the main-secondary connection rib, which leads to the distortion of the bending moment. In addition, the bending moment of the double arch rib is more sensitive to the load than that of the single arch rib. The maximum bending moment occurs at the arch footing on both sides under the four working conditions. The bending moment near the arch rib bifurcation, 1/4 span and 3/4 span of the main arch rib

is small and less affected by the combination of load. It shows that the load changes at the arch rib bifurcation, 1/4 span, and 3/4 span of the main arch rib are mainly borne by the axial force.

- (3) The axial force of the main arch rib is larger on the single arch rib and smaller on the double arch rib. In addition, there is an axial force mutation at the direct connection between the secondary arch rib and the single arch rib or the double arch rib, which match points on the horizontal coordinates of 20 m and 200 m in Fig. 15c. According to the comparison between working condition 1 and working condition 2, it can be found that the axial force of the main arch rib under the live load is 9.7% higher than under the constant load on average. Comparing working condition 2, working condition 3, and working condition 4, it can be seen that the single arch footing is less affected by the temperature. Compared with the single arch footing, the double arch footing is greatly affected by the temperature. The influence of temperature on the axial force of the main arch rib increases gradually from the arch footing to the arch vault, and the temperature load at 7 m from the arch vault has the greatest influence on the axial force of the main arch rib.

4.2 Static Mechanical Properties of the Suspender

The suspenders of the spatial Y-shaped tied arch bridge are asymmetric arrangement, it is also important to study its mechanical properties. The special-shaped arch bridge is a canyon landscape bridge, which has high requirements for suspender arrangement. The suspenders of the single arch rib are arranged as the type of single cable plane double straight suspenders, and the suspenders of double arch rib are arranged as the type of double cable plane single inclined suspenders. Due to the influence of spatial Y-shaped arch rib, the arrangement of suspenders changes from upper-narrow and lower-wide at mid-span to upper-wide and lower-narrow at the double arch seat. The arrangement diagram of

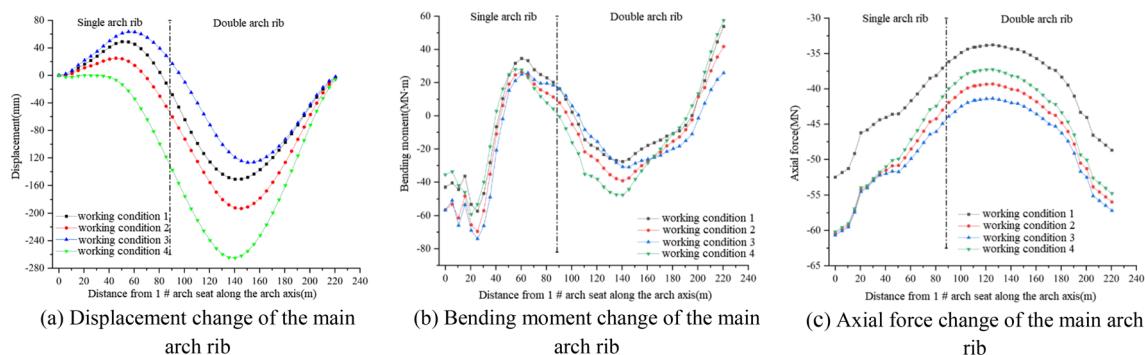


Fig. 15 Calculation results of the main arch rib under four working conditions

suspenders is shown in Fig. 16. The suspender force under different working conditions is shown in Fig. 17.

It can be seen from Fig. 17 that:

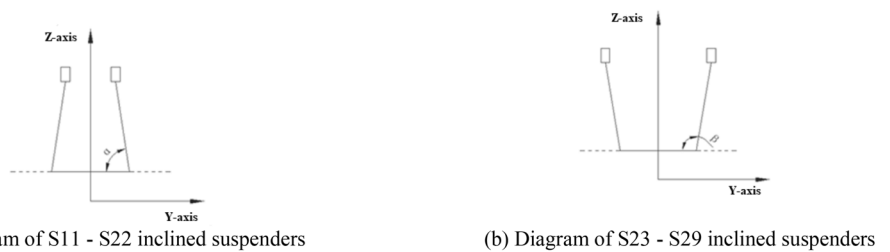
- (1) Under the constant load, the suspender force in the middle of the spatial Y-shaped tied arch bridge is relatively uniform. The force of S1 ~ S10 in the single arch rib is smaller than that of S11 ~ S29 in the double arch rib, and the larger force appears on both sides of the bridge span, which is 1247.8kN. Under the constant load, The suspender force value is about 1/3 of the breaking force value.
- (2) Under the live load, the force around 1/4 span and 3/4 span of the main arch rib are relatively average. The larger force appears on both sides of the bridge span and S14 ~ S17, and the maximum force appears at S15, which is 229.7kN.
- (3) Under the use stage, the suspender force gradually decreases from both sides of the bridge span to the middle, which is similar to the suspender force under the

constant load. The larger force appears on both sides of the bridge span, and the maximum force appears at S1, which is 1468kN.

4.3 Sensitivity Analysis of Rise-Span Ratio on Static Mechanical Properties

The rise-span ratio is the ratio of the calculation arch rise to the calculation span, which is one of the main structural parameters of arch bridges. The rise-span ratio not only affects the internal force of arch bridges but also has a great influence on the selection of bridge construction technology and the adaptation of arch bridges to the surrounding environment. In order to analyze the influence of the rise-span ratio on the internal force of the spatial Y-shaped arch bridge under the constant load (gravity + second constant load) and live load, reference to the *Specifications for Design of Highway Concrete-filled Steel Tubular Arch Bridges (JTG-T D65-06–2015)*, five models with rise-span ratios of 1:4.02, 1:4.52, 1:5.02, 1:5.52, 1:6.02 were established

Fig. 16 The arrangement diagram of suspenders



(a) Diagram of S11 - S22 inclined suspenders

(b) Diagram of S23 - S29 inclined suspenders

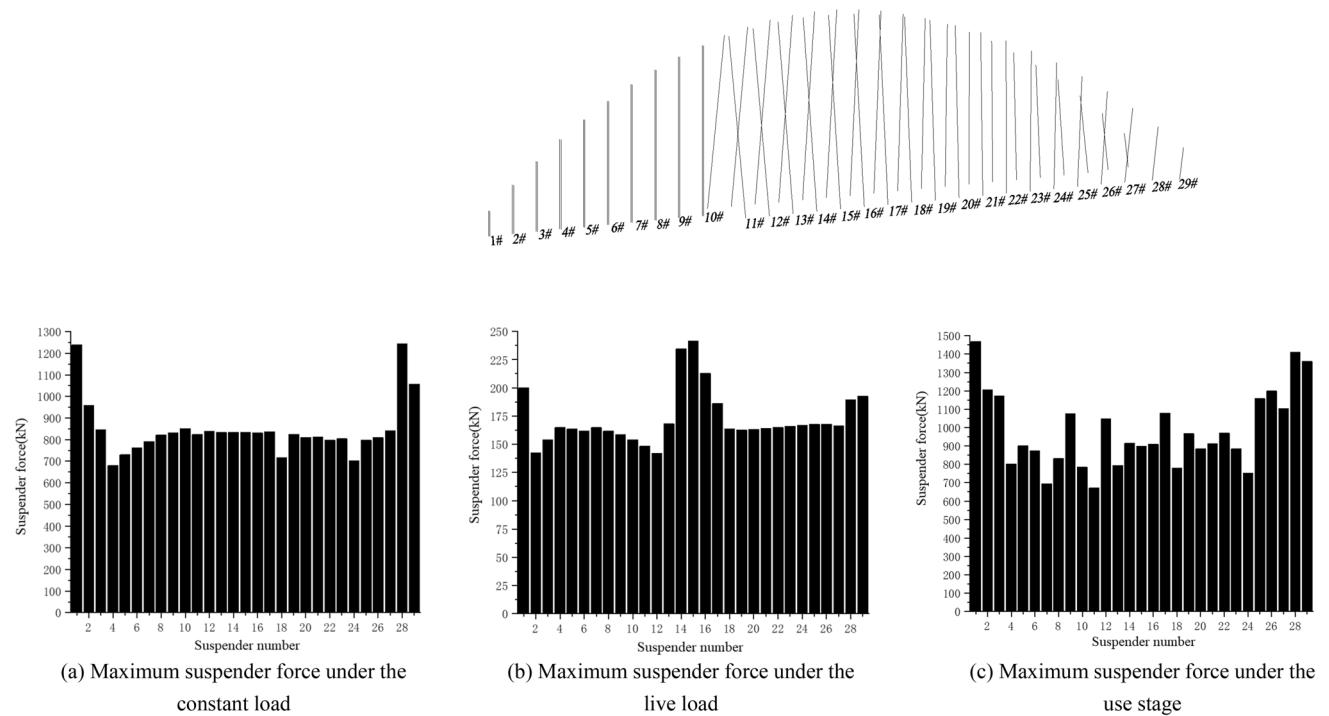


Fig. 17 The suspender force under different working conditions

based on the original bridge rise-span ratio of 1:3.52, and the following assumptions are made: (1) Keep the calculation span unchanged, only adjusting the calculation arch rise to make the rise-span ratio in 1:4.02~1:6.02; (2) Keep the arch axis equation unchanged, the size of main arch rib section is unchanged, The load and boundary conditions don't change.

After calculation, the selected five models can meet the structural design requirements. The axial force and bending moment of the main arch rib under different rise-span ratios under the constant load and the live load are calculated. In order to facilitate the comparative analysis of the result of

different rise-span ratios, based on the internal force value under the rise-span ratio of 1:3.52, the internal force values under other rise-span ratios are unitized to obtain the internal force change diagram of the main arch rib, as shown in Figs.18, 19.

It can be seen from Fig. 18 that:

- (1) Under the constant load, the axial force of the main arch rib gradually increases with the decrease of the rise-span ratio, and the influence of the rise-span ratio on the axial force of the main arch rib decreases from the

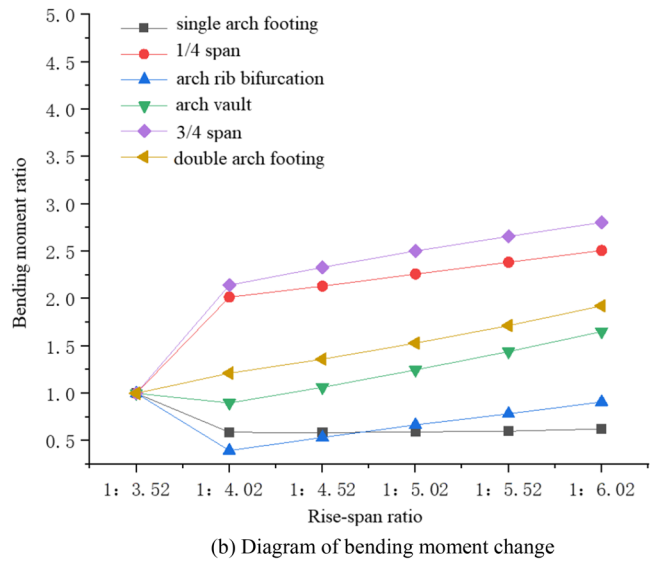
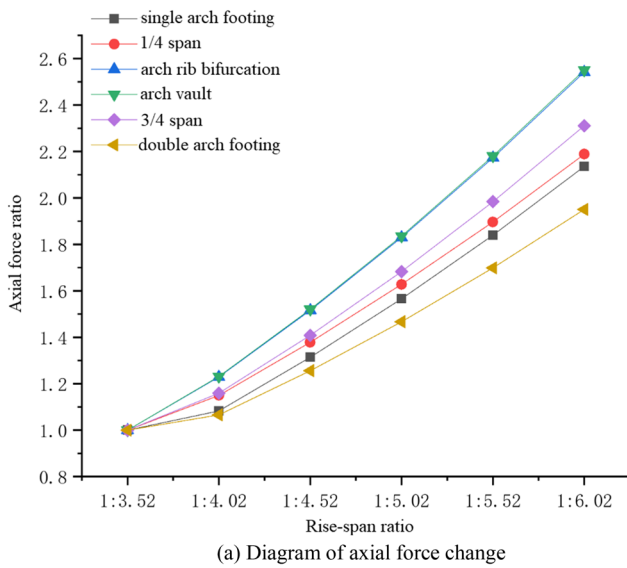


Fig. 18 Change of the internal force of main arch rib under the constant load

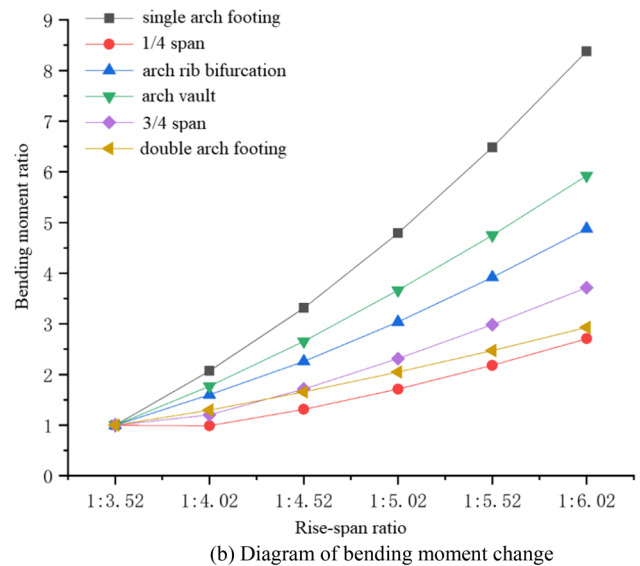
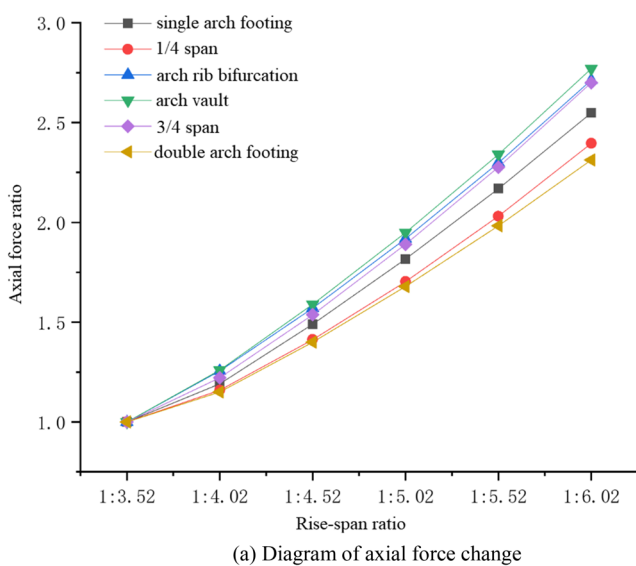


Fig. 19 Change of the internal force of main arch rib under the live load

arch vault to the arch footing. When the rise-span ratio changes from 1:3.52 to 1:6.02, the maximum increase of axial force appears at the arch vault and the arch rib bifurcation. The axial force changes at the arch vault and the arch rib bifurcation are basically the same. When the rise-span ratio is 1:6.02, the axial force at the arch rib bifurcation is 1.6 times larger than that at the arch rib bifurcation of the original bridge.

- (2) Under the constant load, the variation trend of the bending moment of the main arch rib is different. The bending moment at the single arch footing and the arch rib bifurcation decreases with the decrease of the rise-span ratio. When the rise-span ratio decreases from 1:3.52 to 1:6.02, the bending moment at the single arch footing decreases by 37.67%, and the bending moment at the arch rib bifurcation reaches the minimum when the rise-span ratio is 1:4.02, and then increases with the decrease of the rise-span ratio. The bending moments of the other part of the arch rib increase with the decrease of the rise-span ratio and the bending moment of the main arch rib which is most affected by the rise-span ratio under constant load are located at the 1/4 span and the 3/4 span.

It can be seen from Fig. 19 that:

- (1) Under live load, the axial force of the main arch rib gradually increases with the decrease of rise-span ratio, and the increase of axial force at the arch vault is the largest, followed by the arch rib bifurcation and the 3/4 span, and the change at the double arch footing is the smallest.
- (2) With the decrease in the rise-span ratio of the main arch rib, the variation trend of the bending moment of each part of the main arch rib under the live load is opposite to that under the constant load. From the rise-span ratio of the original bridge to 1:6.02, the bending moment at the single arch footing is the most affected by the change of the rise-span ratio under the live load. With the decrease of the rise-span ratio, the bending moment at the single arch footing increases by 7.38 times, and the bending moment at the 1/4 span is the least affected by the change of the rise-span ratio, only increasing by 1.2 times.

4.4 Sensitivity Analysis of Bifurcation Angle on Static Mechanical Properties

The main arch rib changes from the single arch rib to the double arch rib in the middle span, forming a spatial special-shaped arch bridge. The angle of the single arch rib divided into double arch ribs into both sides is called the bifurcation angle of the double arch rib. The bifurcation

angle is one of the important structural parameters of the special-shaped arch bridge, which not only directly affects the linear landscape of the bridge, but also has an important impact on the internal force and stability of the arch rib. In order to analyze the influence of the bifurcation angle on the internal force of the spatial Y-shaped arch bridge under the constant load (gravity + second constant load) and live load, based on some similar Y-shaped bridge experiments (Li et al., 2015a, 2015b, 2016; Yan & Li, 2017; Yan et al., 2016), five models with bifurcation angles of 15°, 17°, 19°, 21° and 23° established based on the original bridge bifurcation angle of 12.42°, and the following assumptions are made: (1) Keep the calculation span and the main beam width unchanged, only changing the bifurcation angle; (2) Keep the arch axis equation, the main arch section size, and the load and boundary conditions unchanged.

After calculation, the selected five models can meet the structural design requirements. The axial force and bending moment of the main arch rib under different bifurcation angles under the constant load and the live load are calculated. In order to facilitate the comparative analysis of the result of different bifurcation angles, based on the internal force value under the bifurcation angle of 12.42°, the internal force values under other bifurcation angles are unitized to obtain the internal force change diagram of the main arch rib, as shown in Figs. 20, 21.

It can be seen from Fig. 20 that:

- (1) Under the constant load, the axial force of the main arch rib is proportional to the change in bifurcation angle. The axial force at the arch vault increases the most, and the angle increases from 12.42° to 23°. The axial force at the arch vault increases by 23.82%, followed by the 3/4 span. The axial force at the double arch footing decreases to the minimum at 15°, which is only 92.33% of the axial force at the original angle. The change of bifurcation angle has little effect on the axial force at the single arch footing.
- (2) Under the constant load, with the increase of the bifurcation angle, the bending moment at the arch vault and the arch rib bifurcation also gradually increases. When the bifurcation angle is 23°, the bending moment increases by 78%. With the increase of the bifurcation angle from 12.42° to 17°, the bending moment at the 3/4 span gradually decreases to 0, and it is affected by the bifurcation angle increasingly. When the bifurcation angle increases from 17° to 19°, the tensile zone and the compression zone at the 3/4 span have changed compared with the original bifurcation angle. Under the constant load, the bending moment at the single arch footing is less affected by the increase of the bifurcation angle. The bending moment at the double arch footing

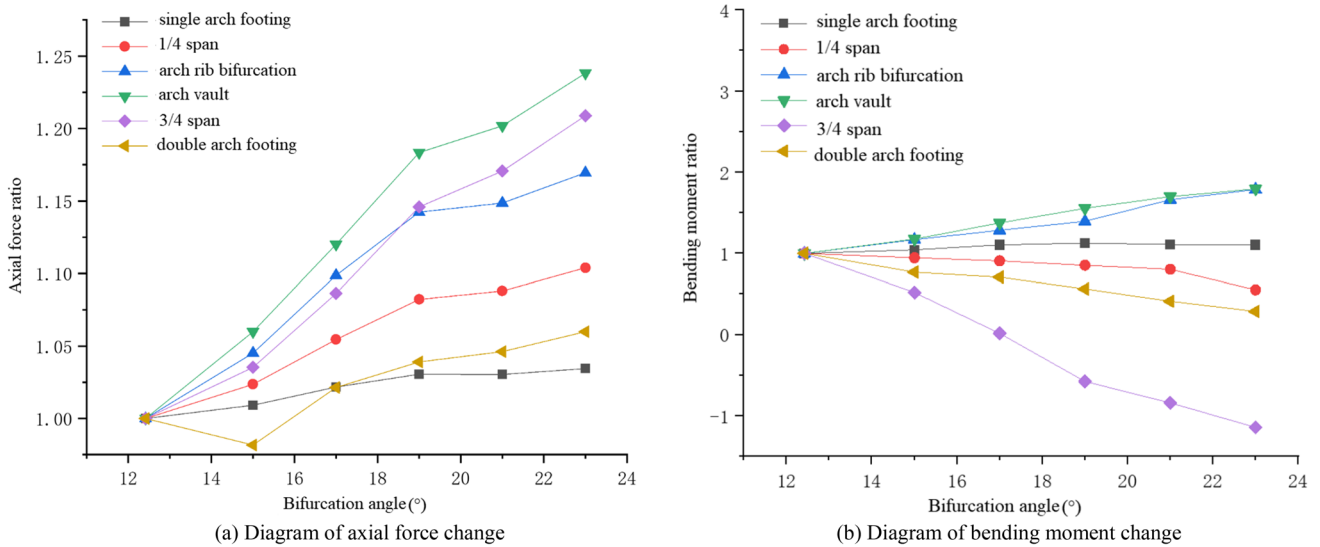


Fig. 20 Change of the internal force of main arch rib under the constant load

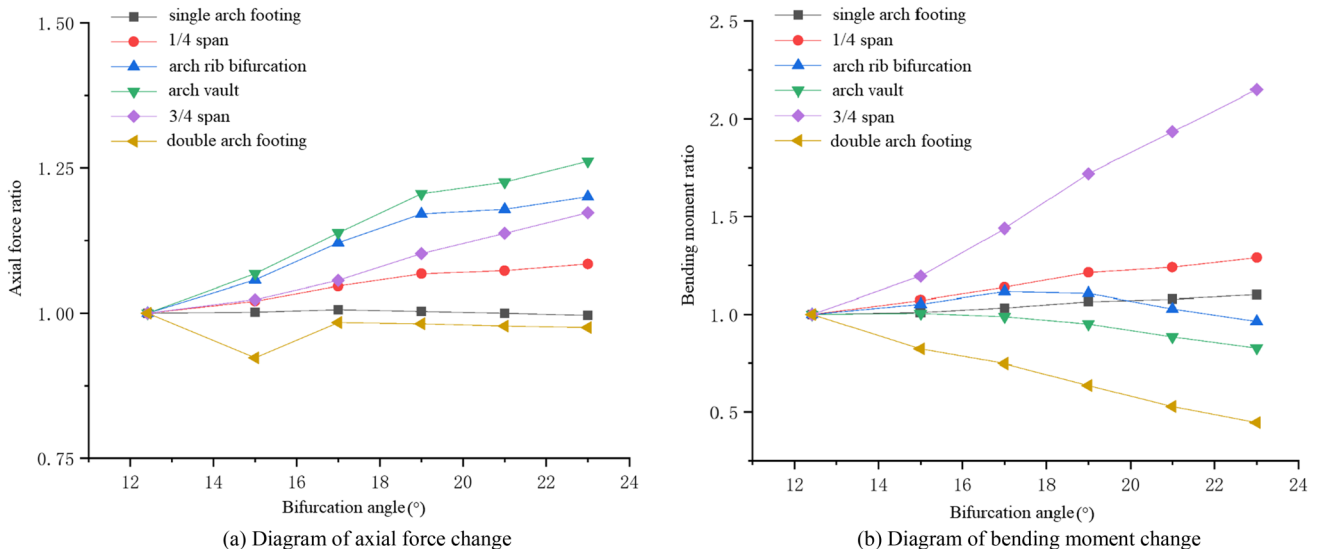


Fig. 21 Change of the internal force of main arch rib under the live load

and the bending moment at the 1/4 span decrease with the increase of the bifurcation angle.

It can be seen from Fig. 21 that:

- (1) Under live load, the axial force at the 1/4 span, the 3/4 span, the arch rib bifurcation, and the arch vault increases with the increase of the bifurcation angle, The axial force at the arch vault is most affected by the change of the bifurcation angle, and the maximum increase is 26.18%. The axial force at the single arch footing and the double arch footing are less affected by the change of the bifurcation angle. The bifurca-
- (2) With the increase of bifurcation angle, the bending moment of the arch vault, arch rib bifurcation, and double arch footing under live load decreases gradually, and the bending moment of double arch footing decreases by 55.53%. The bending moment at the arch rib bifurcation is proportional to the bifurcation angle from 12.42° to 15°, but as the bifurcation angle continues to increase, the bending moment at the arch rib

bifurcation is inversely proportional to it. The bending moment at the 1/4 span and the 3/4 span increases with the increase of the bifurcation angle. The bending moment at the 3/4 span is most affected by the change of the bifurcation angle, and the growth rate is 114.9% compared with the original bridge.

5 Dynamic Mechanical Properties and Parameter Sensitivity of the Spatial Y-shaped Tied Arch Bridge

5.1 Dynamic Characteristics of the Spatial Y-Shaped Tied Arch Bridge

The dynamic characteristics of the spatial Y-shaped tied arch bridge are analyzed by using the subspace iteration method of the characteristic equation in Midas Civil (Gou et al., 2018; Roeder et al., 2000). In general structural dynamic analysis, the first several orders of natural frequencies and vibration modes play a control role, so the first 6 orders of natural frequencies and vibration modes are selected, and the results are shown in Table 3.

From Table 3, the following natural vibration characteristics of the spatial Y-shaped tied arch bridge can be obtained:

- (1) The spatial Y-shaped tied arch bridge has two forms of deflection vibration and bending-torsion vibration. It can be seen from the vibration mode that the spatial Y-shaped tied arch bridge has good structural integrity (Min & Santos, 2017).
- (2) The basic frequency of this bridge is 0.7749 Hz, and the corresponding vibration mode is transverse deflection vibration of arch rib, which belongs to moderate flexibility structures.
- (3) The first order frequency of bending-torsion vibration of the arch rib is 1.434 Hz, which is 1.85 times the first order frequency of deflection vibration of the arch

rib. The natural vibration characteristics of the arch rib are mainly deflection vibration. It shows that the bending-torsion stability of the spatial Y-shaped tied arch bridge is higher than that of the deflection stability. In the design, more attention should be paid to the deflection stability of the arch rib.

- (4) The arch rib has better torsional stability. The main reasons are as follows: The three arch ribs constitute a stable tetrahedral spatial structure. The suspenders between the arch rib and the main beam are arranged in space. There are wind braces and cross beams between the double arch rings to strengthen the transverse connection, so the torsion stiffness of the spatial Y-shaped tied arch bridge is large.
- (5) In the first six-order natural vibration characteristics, the main beam is dominated by vertical deflection vibration, and only one bending-torsion vibration occurs in the main beam with a frequency of 1.7322 Hz, indicating that the main beam has high bending-torsion stability. Due to the connection effect of suspenders, the arch rib and the main beam have the characteristics of synchronous vibration in vertical deflection.
- (6) In the case of only the main arch rib, secondary arch rib, main-secondary arch connecting rib, and wind brace, the basic frequency is 0.7327 Hz, accounting for 94.55% of the basic frequency of the whole bridge, indicating that the main arch rib and the secondary arch rib contribute greatly to the overall stiffness of the bridge.

The first six-order vibration mode diagram of the spatial Y-shaped tied arch bridge is shown in Fig. 22.

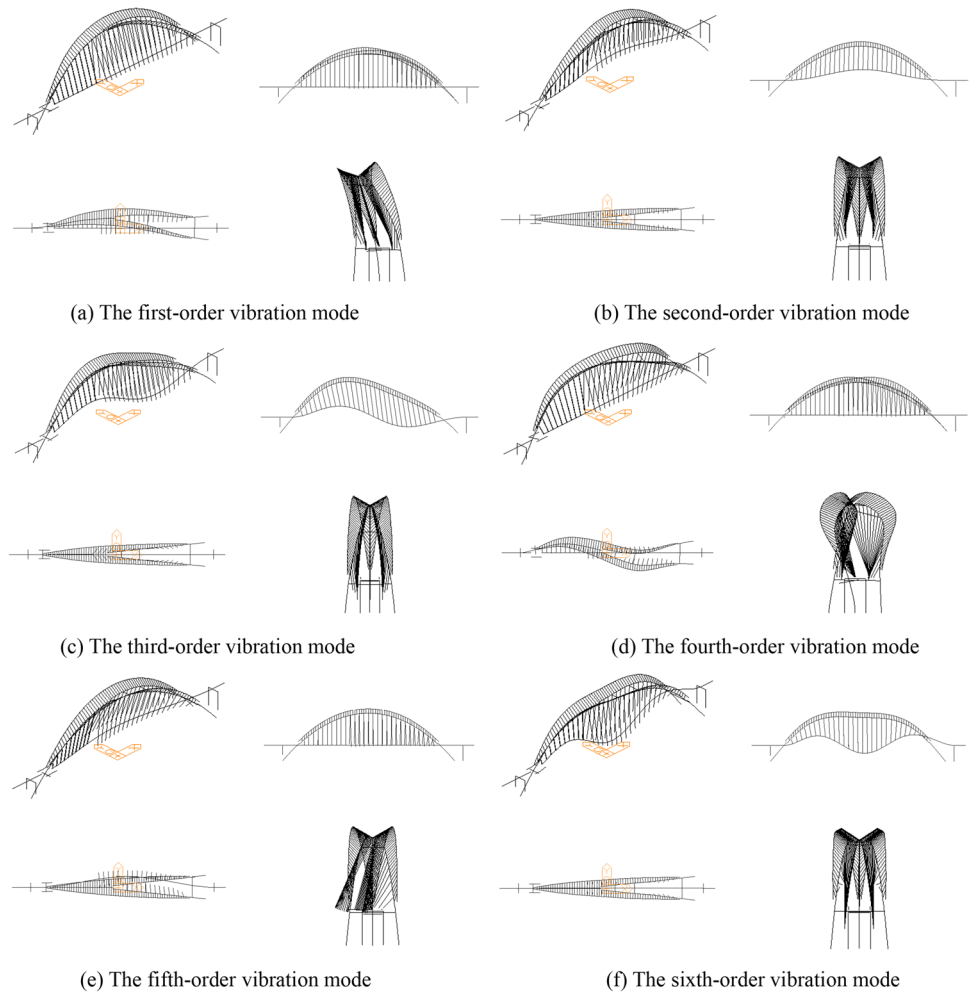
5.2 Sensitivity Analysis of Rise-Span Ratio on Dynamic Mechanical Properties

As the main parameter of arch bridges, the rise-span ratio will also have an impact on the dynamic characteristics of

Table 3 Calculation results of natural vibration characteristics of the spatial Y-shaped tied arch bridge

Vibration mode	Natural frequency/Hz	Modal characteristics	Vibration mode	Natural frequency/Hz	Modal characteristics
1	0.774942	Transverse deflection vibration of the arch rib	4	1.433978	Antisymmetric transverse bending-torsion vibration of the arch rib
2	0.899334	Vertical deflection vibration of the arch rib; Vertical deflection vibration of the main beam	5	1.732228	Transverse bending-torsion vibration of the main beam
3	1.033654	Vertical deflection vibration of the arch rib; Antisymmetric vertical deflection vibration of the main beam	6	1.778235	Vertical deflection vibration of the arch rib;xxxVertical symmetrical deflection vibration of the main beam

Fig. 22 The first six-order vibration mode diagram of the spatial Y-shaped tied arch bridge



the bridge, the study of the rise-span ratio on the dynamic characteristics of the bridge is also very important. Based on the parameters and assumptions in Sect. 4.3.

In this section, this paper studies the influence of the rise-span ratio on the dynamic characteristics mainly by comparing the natural frequencies of the first deflection vibration and the first bending-torsion vibration of the main arch rib or the main beam under different rise-span ratios. For the convenience of comparative analysis, based on the natural frequency value under the rise-span ratio of 1:3.52, the natural frequency values under other rise-span ratios are unitized to obtain the natural frequency change diagram of the bridge, as shown in Fig. 23.

According to the calculation results and Fig. 23, it can be seen that:

- (1) The first-order natural frequencies of the four vibration modes of the bridge decrease with the decrease of the rise-span ratio, the most affected by the decrease of the rise-span ratio is the bending-torsion vibration of the arch rib, which decreases by 63%. The main rea-

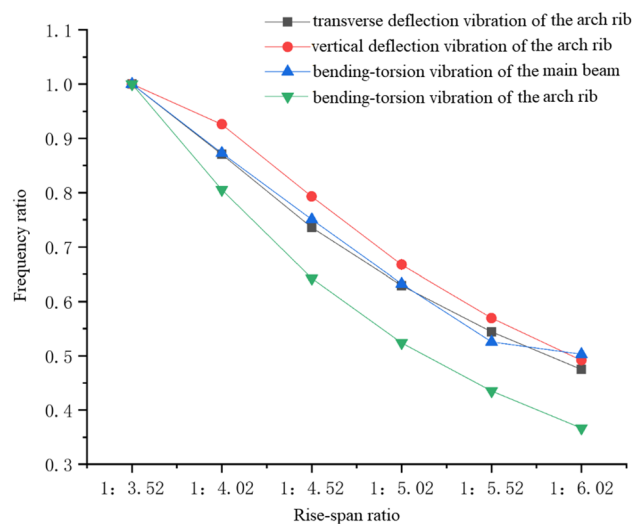


Fig. 23 Vibration frequency ratio under different rise-span ratios

son for this phenomenon is that the spatial structure of the tetrahedral structure composed of the main arch rib gradually flattens with the decrease of the rise-span ratio, which reduces the lateral stiffness of the main arch rib.

- (2) The frequency of the bending-torsion vibration of the main beam is reduced by 48.7% when the rise-span ratio is 1:3.52 compared with 1:5.52, but it is only reduced by 3.32% when the rise-span ratio is 1:5.52 to 1:6.02, indicating that when the rise-span ratio is reduced to 1:5.52, the influence of the change of the rise-span ratio on the stiffness of the main beam is also gradually reduced. As the rise-span ratio decreases, the frequency corresponding to the deflection vibration of the arch rib decreases by 52.51%.

Through the analysis, it can be concluded that the change in the rise-span ratio has a great influence on the natural vibration characteristics of the bridge, and the decrease in the rise-span ratio leads to the decrease in stiffness of the arch bridge. The bending-torsion stiffness of the main arch rib is the most affected by the rise-span ratio, followed by the bending-torsion stiffness of the main beam, but when the rise-span ratio is reduced to 1:5.52, the impact on the stiffness of the main beam is also getting smaller.

5.3 Sensitivity Analysis of Bifurcation Angle on Dynamic Mechanical Properties

As the main parameter of arch bridges, the bifurcation angle will also have an impact on the dynamic characteristics of the bridge, the study of the bifurcation angle on the dynamic characteristics of the bridge is also very important. Based on the parameters and assumptions in Sect. 4.4.

In this section, this paper studies the influence of bifurcation angle on the dynamic characteristics mainly by comparing natural frequencies of the first deflection vibration and the first bending-torsion vibration of the main arch rib or the main beam under different bifurcation angles. For the convenience of comparative analysis, based on the natural frequency value under the bifurcation angle of 12.42° , the natural frequency values under other bifurcation angles are unitized to obtain the natural frequency change diagram of the bridge, as shown in Fig. 24.

According to the calculation results and Fig. 24, it can be seen that:

- (1) The frequency of transverse deflection vibration of the arch rib is most affected by the increase in bifurcation angle, when the bifurcation angle increases to 23° , the transverse deflection vibration frequency of the arch rib increases by 33.45% compared with that of the original bifurcation angle of 12.42° . The main reason is that

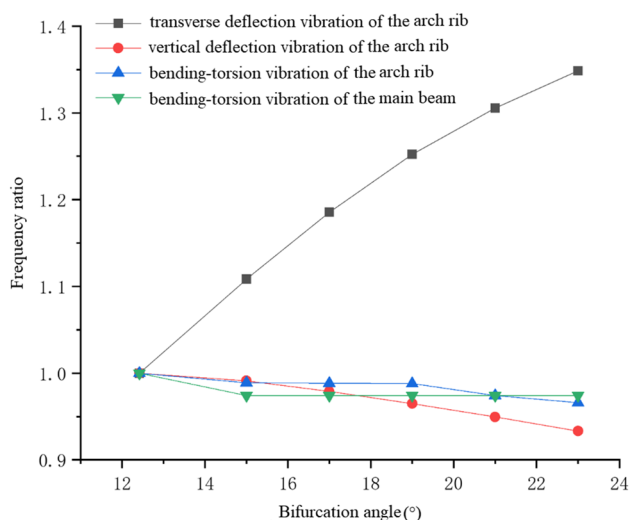


Fig. 24 Vibration frequency ratio under different bifurcation angles

with the increase of the bifurcation angle, the tetrahedral structure composed of the main arch rib tends to be plumper, which increases the structural stiffness.

- (2) The frequency of the vertical deflection vibration of the arch rib, the bending-torsion vibration of the main beam, and the bending-torsion vibration of the arch rib are less affected by the bifurcation angle. The three frequencies decrease slightly with the increase of the bifurcation angle, and the decrease is only about 1.4% compared with the original bridge.

Through the analysis, it can be seen that the change of the bifurcation angle only has a significant effect on the stiffness of the arch rib. When the bifurcation angle is increased, the transverse deflection stiffness of the arch rib is greatly improved, but the stiffness of the main beam and the longitudinal and vertical stiffness of the main arch rib are little affected by the change of the bifurcation angle.

6 Conclusion

A novel spatial Y-shaped tied arch bridge is proposed in this paper, this paper introduces the bridge engineering and model building briefly and analyzes the static and dynamic performance of this bridge under different load combinations and the influence of different structural parameters on mechanical properties. As a study of a new type of special-shaped arch bridge, the analysis results have great reference significance for the design of the special-shaped arch bridge in the future. The conclusions are summarized as follows:

- (1) Under the constant load, live load, and temperature effect, the arch rib of the bridge are mainly under axial

compression. The overall change of the axial force is relatively gentle, which is greatly affected by the live load and temperature change, about 10.8%. Under each load combination, the axial force of the single arch rib is 8.3% larger than that of the double arch rib. The displacement of the double arch rib under the combined load is increased by at least 37.5% compared with that of the single arch rib, the main reason is that the horizontal component force produced by the double arch inclined suspender and the double arch rib is greater than the that of the single arch rib when the cross-sectional dimensions of the single arch rib and the double arch rib are similar.

- (2) Under the constant load, the suspender force of the inclined suspender at the double arch footing increases by 45.3% compared with that at the arch vault of the bridge. The suspender force of the single arch has obvious changes, and that of the double arch rib has little change. Under the live load, there is a large concentrated load in the arch vault, which makes the suspender force decrease from the arch vault to the arch footing. It can be seen that the variation trend of the straight suspender force of the single arch rib is similar to that of the ordinary tied arch bridge. With the change of the angle of the suspender, the force of the double arch rib inclined suspender decreases first and then increases due to the influence of the horizontal component force.
- (3) The change of the rise-span ratio has a great influence on the internal force of the single arch rib, and the axial force and bending moment increase with the decrease of the rise-span ratio. The change of the bifurcation angle has a great influence on the internal force of the double arch rib. The axial force and bending moment increase gradually with the increase of the bifurcation angle. These results can provide a reference for bridge optimization in the future.
- (4) The spatial system stiffness of the spatial Y-shaped arch tied bridge composed of the single arch rib, double arch rib, straight suspender, and inclined suspender is relatively large, and it has high bending-torsion stability. The decrease in the rise-span ratio makes the structural stiffness of the arch bridge decrease gradually, and the maximum reduction of the frequency of the arch rib bending-torsion vibration is 63%. The change of the bifurcation angle only has a significant effect on the transverse stiffness of the arch rib of the bridge, and the torsion stiffness is almost not affected by the change of the bifurcation angle. In general, the spatial Y-shaped tied arch bridge has good structural integrity.

Acknowledgements The financial support of Xi'an Science and technology innovation talent service enterprise project (Grant

Nos.2020KJRC0047), Natural Science Foundation of Shaanxi Province (Grant Nos.2020JM-475) and National Natural Science Foundation of China (Grant Nos.51408453) are much appreciated.

Declarations

Conflict of interests The authors declare that they have no known competing financial interests or personal relationships that could have influenced the work reported in this paper.

References

- Backer, H. D., Outtier, A., & Bogaert, P. V. (2014). Buckling design of steel tied-arch bridges. *Journal of Constructional Steel Research*, 103, 159–167. <https://doi.org/10.1016/j.jcsr.2014.09.004>
- Banerji, P., & Chikermane, S. (2012). Condition assessment of a heritage arch bridge using a novel model updation technique. *Journal of Civil Structural Health Monitoring*, 2, 1–16. <https://doi.org/10.1007/s13349-011-0013-9>
- Batista, E., & Ghavami, K. (2005). Development of brazilian steel construction. *Journal of Constructional Steel Research*, 61(8), 1009–1024. <https://doi.org/10.1016/j.jcsr.2005.02.011>
- Chen, B. C., & Wang, T. L. (2009). Overview of concrete filled steel tube arch bridges in China. *Practice Periodical on Structural Design & Construction*, 14(2), 70–80. [https://doi.org/10.1061/\(ASCE\)1084-0680\(2009\)14:2\(70\)](https://doi.org/10.1061/(ASCE)1084-0680(2009)14:2(70))
- Cheng, X. X., Dong, J., Cao, S. S., Han, X. L., & Miao, C. Q. (2017). Static and dynamic structural performances of a special-shaped concrete-filled steel tubular arch bridge in extreme events using a validated computational model. *Arabian Journal for Science & Engineering*, 43, 1839–1863. <https://doi.org/10.1007/s13369-017-2771-0>
- Cheng, C., Xie, X., & Yu, W. (2021). Investigation of the fatigue stress of orthotropic steel decks based on an arch bridge with the application of the arlequin method. *Materials*, 14(24), 7653. <https://doi.org/10.3390/ma14247653>
- Fan, J., Xiao, Z., & Cheng, X. (2022). Numerical simulations of modal tests on Yingzhou Bridge using a passing vehicle as the excitation. *Experimental Techniques*, 46, 529–541. <https://doi.org/10.1007/s40799-021-00484-y>
- Feng, Y., Wang, C., Briseghella, B., Fenu, L., & Zordan, T. (2021). Structural Optimization of a Steel Arch Bridge with Genetic Algorithm. *Structural Engineering International*, 31(3), 347–356. <https://doi.org/10.1080/10168664.2020.1773373>
- Gou, H., Zhou, W., Chen, G., Bao, Y., & Pu, Q. (2018). In-situ test and dynamic response of a double-deck tied-arch bridge. *Steel and Composite Structures*, 27(2), 161–175. <https://doi.org/10.12989/scs.2018.27.2.161>
- He, W., & Chen, H. (2014). Characteristics and related research of through and half through arch bridges in China. *Applied Mechanics & Materials*, 488–489, 509–512. <https://doi.org/10.4028/www.scientific.net/AMM.488-489.509>
- Huang, Q., Wu, X., Wei, H., & Chen, Q. (2022). innovative design of novel main and secondary arch collaborative Y-shaped arch bridge and research on shear lag effect of its unconventional thin-walled steel box arch ribs. *Applied Sciences*, 12, 8370. <https://doi.org/10.3390/app12168370>
- Huo, X. J., & Han, L. Z. (2014). Analysis of geometric nonlinearity of special-shaped arch bridges. *Journal of Highway & Transportation Research & Development*, 8(3), 37–45. <https://doi.org/10.3969/j.issn.1002-0268.2013.07.009>
- Jin, C., & Li, Q. S. (2009). Reliability analysis of a long span steel arch bridge against wind-induced stability failure during construction.

- Journal of Constructional Steel Research*, 65(3), 552–558. <https://doi.org/10.1016/j.jcsr.2008.07.019>
- JTG D64-2015 (2015). Specification for design of highway steel bridge. Ministry of transport of the people's Republic of China.
- JTG/T D65-06-2015 (2015). Specifications for design of highway concrete-filled steel tubular arch bridges. Ministry of transport of the people's Republic of China.
- Kasimzade, A. A., Tuhta, S., Furkan, G., & Aydn, H. (2021). Obtaining dynamic parameters by using ambient vibration recordings on model of the steel arch bridge. *Periodica Polytechnica Civil Engineering*, 65(2), 608–618. <https://doi.org/10.3311/PPci.16422>
- Kou, C. H., Huang, Y. Z., Yang, G., Ma, S. W., & Wu, T. T. (2011). An investigation into the static mechanical behaviors of special-shaped arch bridge. *Advanced Materials Research*, 382, 289–292. <https://doi.org/10.4028/www.scientific.net/AMR.382.289>
- Li, C., Zeng, G., & Liu, Y. (2004). Determination of reasonable construction states of special-shaped tied-arch bridge with full framing. *Iabse Symposium Report*, 88(6), 373–378. <https://doi.org/10.2749/222137804796291430>
- Li, Q. N., Yin, J. H., Yan, L., Cheng, M. L., & Li, W. (2015a). Shaking table tests for a Y-shape bridge under multi-dimensional earthquake excitation. *Journal of Vibration Shock*, 34(15), 103–108. <https://doi.org/10.13465/j.cnki.jvs.2015.15.019>. (in Chinese).
- Li, Q., Cheng, M., Yin, J., & Zhou, C. (2016). Study on seismic disaster mechanism of irregular C-shaped curved bridge with high piers. *KSCE Journal of Civil Engineering*, 20, 1429–1436. <https://doi.org/10.1007/s12205-015-0649-9>
- Li, J., Tao, C., & Qin, H. (2018). Analysis of triangular frame prestressed and tuspender force on mechanical behavior of V pier special-shaped steel composite beam arch composite bridge. *Journal of Zhengzhou University (natural Science Edition)*, 50(1), 116–122. <https://doi.org/10.13705/j.issn.1671-6841.2017231>. (in Chinese).
- Li, C., Wu, L. L., Chai, S., Zhao, Y., & Zhou, Y. J. (2020). Analysis of the influence of boundary conditions on the mechanical characteristics of arch bridge with composite arch. *IOP Conference Series Earth and Environmental Science*, 446, 052035. <https://doi.org/10.1088/1755-1315/446/5/052035>
- Li, Y., Zha, X., & Zhu, C. (2015b). Shenzhen bay flying swallow type composite arch bridge design. *Proceedings of the 2nd International Conference on Civil Materials and Environmental Sciences*. <https://doi.org/10.2991/cmcs-15.2015.19>
- Liu, A. R., Huang, Y. H., Yu, Q. C., & Rao, R. (2014a). An analytical solution for lateral buckling critical load calculation of leaning-type arch bridge. *Mathematical Problems in Engineering*, 2014(2014), 1–14. <https://doi.org/10.1155/2014/578473>
- Liu, W., Guo, H., Li, H., & Li, Y. (2014b). Using BIM to improve the design and construction of bridge projects: A case study of a long-span steel-box arch bridge project regular paper. *International Journal of Advanced Robotic Systems*, 11, 125. <https://doi.org/10.5772/58442>
- Liu, B., Wang, Y., Hu, P., & Yuan, Q. (2015). Impact coefficient and reliability of mid-span continuous beam bridge under action of extra heavy vehicle with low speed. *Journal of Central South University*, 22(4), 1510–1520. <https://doi.org/10.1007/s11771-015-2668-6>
- Lonetti, P., Pascuzzo, A., & Aiello, S. (2018). Instability design analysis in tied-arch bridges. *Mechanics of Advanced Materials and Structures*. <https://doi.org/10.1080/15376494.2017.1410911>
- Lu, P., Zhang, J., & Zhao, R. (2009). Study on the mechanical performance of butterfly arch bridge. *The Structural Design of Tall and Special Buildings*, 18, 469–483. <https://doi.org/10.1002/tal.449>
- Lu, P., Zhang, J., Li, D., Zhou, Y., & Shi, Q. (2021). Conceptual design and experimental verification study of a special-shaped composite arch bridge. *Structures*, 29(1), 1380–1389. <https://doi.org/10.1016/j.istruc.2020.12.018>
- Ma, Y., Zhang, Y., Han, Q., Wang, F., Jiang, Y., & Li, H. (2021). Internal force calculation of half through arch bridge based on elastic foundation beam algorithm. *International Conference on Smart Transportation and City Engineering*, 2021, 12050R. <https://doi.org/10.1117/12.2614420>
- Min, X., & Santos, L. O. (2017). Dynamic assessment of the São João bridge structural integrity. *Procedia Structural Integrity*, 5, 325–331. <https://doi.org/10.1016/j.prostr.2017.07.178>
- Nonaka, T., & Ali, A. (2001). Dynamic response of half-through steel arch bridge using fiber model. *Journal of Bridge Engineering*, 6(6), 482–488. [https://doi.org/10.1061/\(ASCE\)1084-0702\(2001\)6:6\(482\)](https://doi.org/10.1061/(ASCE)1084-0702(2001)6:6(482))
- Qin, S., Feng, J., Zhou, Y., Li, C., Huo, X., Figueiredo, E., & Yang, F. (2022). Investigation on the dynamic impact factor of a concrete filled steel tube butterfly arch bridge. *Engineering Structures*, 252, 113614. <https://doi.org/10.1016/j.engstruct.2021.113614>
- Roeder, C. W., Macrae, G., & Crocker, P. (2000). Dynamic response and fatigue of steel tied-arch bridge. *Journal of Bridge Engineering*, 5(1), 14–21. [https://doi.org/10.1061/\(ASCE\)1084-0702\(2000\)5:1\(14\)](https://doi.org/10.1061/(ASCE)1084-0702(2000)5:1(14))
- Shi, Z., Hu, H., & Li, J. (2020). Axis optimisation of arch-shaped pylons for high-speed railway cable-stayed bridges. *Engineering Structures*, 227, 111424. <https://doi.org/10.1016/j.engstruct.2020.111424>
- Sun, J., Zhang, J., Huang, W., Zhu, L., Liu, Y., & Yang, J. (2020). Investigation and finite element simulation analysis on collapse accident of Heyuan Dongjiang Bridge. *Engineering Failure Analysis*, 115104655–S135063071931653X 104655. <https://doi.org/10.1016/j.engfailanal.2020.104655>
- Sun, J., & Tan, Z. (2022). Seismic resilience-based design method for hybrid bridge pier under four-level seismic fortifications. *International Journal of Steel Structures*, 22(5), 1578–1593.
- Sun, J., & Zhufu, G. (2022). Mechanical behavior of laminated rubber isolation bearing with buckling steel plate. *International Journal of Steel Structures*, 22(4), 1069–1085. <https://doi.org/10.1007/s13296-022-00623-0>
- Sun, J., Liu, K., Liu, G., & Li, H. (2021). A developed transfer matrix method for analysis of elastic–plastic behavior of structures. *International Journal of Steel Structures*, 21(5), 1620–1629. <https://doi.org/10.1007/s13296-021-00524-8>
- Sun, J., Jiang, Y., Lv, G., Liu, K., & Zhao, J. (2022a). Simulation analysis on seismic performance of assembled composite energy dissipation pipe joint. *International Journal of Steel Structures*, 22(3), 880–893. <https://doi.org/10.1007/s13296-022-00611-4>
- Sun, J., Qu, X., & Gao, C. (2022b). Study on the design method of ring groove rivet joint in aluminum alloy structure. *International Journal of Steel Structures*, 22(1), 294–307. <https://doi.org/10.1007/s13296-021-00575-x>
- Sun, J., Lv, G., & Ma, X. (2022c). An improved typhoon simulation method based on Latin hypercube sampling method. *Scientific Reports*, 12(1), 9313.
- Sun, J., Li, J., Jiang, Y., Ma, X., Tan, Z., & Zhufu, G. (2022d). Key construction technology and monitoring of long-span steel box tied arch bridge. *International Journal of Steel Structures*. <https://doi.org/10.1007/s13296-022-00687-y>
- Sui, W., Li, H., Zhang, Q., Wang, Z., & Jin, X. (2020). The mechanical properties of a new corrugated steel plate damper and its application in a steel arch bridge. *Structural Engineering*, 24, 228–240. <https://doi.org/10.1007/s12205-020-0888-2>
- Svensden, B. T., Petersen, Y. W., Frseth, G. T., & Rnnquist, A. (2021). Improved finite element model updating of a full-scale steel bridge using sensitivity analysis. *Structure and Infrastructure Engineering*. <https://doi.org/10.1080/15732479.2021.1944227>
- Tabar, A. M., Domenico, D. D., & Dindari, H. (2021). Seismic rehabilitation of steel arch bridges using nonlinear viscous dampers: Application to a case study. *Practice Periodical on Structural*

- Design and Construction*, 26(3), 04021012. [https://doi.org/10.1061/\(ASCE\)SC.1943-5576.0000576](https://doi.org/10.1061/(ASCE)SC.1943-5576.0000576)
- Tang, C., Zheng, L., & Zhang, Z. (2014). Construction controls for a half-through tied arch bridge in China. *Structural Engineering International*, 24(4), 557–561. <https://doi.org/10.2749/101686614X13854694314766>
- Tubaldi, E., Macorini, L., & Izzuddin, B. A. (2019). Identification of critical mechanical parameters for advanced analysis of masonry arch bridges. *Structure and Infrastructure Engineering*, 16(2), 328–345. <https://doi.org/10.1080/15732479.2019.1655071>
- Wang, H., Jiang, R., & Pan, Z. (2011). Design and analysis of slanting cross special-shaped arch bridge. *Advanced Materials Research*, 255–260, 786–791. <https://doi.org/10.4028/www.scientific.net/AMR.255-260.786>
- Wang, H., Tao, T., Zhou, R., Hua, X., & Kareem, A. (2014). Parameter sensitivity study on flutter stability of a long-span triple-tower suspension bridge. *Journal of Wind Engineering and Industrial Aerodynamics*, 128, 12–21. <https://doi.org/10.1016/j.jweia.2014.03.004>
- White, D., & Fortune, J. (2012). Using systems thinking to evaluate a major project: The case of the gateshead millennium bridge. *Engineering*, 19(2), 205–228. <https://doi.org/10.1108/0969998121206124>
- Wu, H. J., & Qiu, W. L. (2012). Dynamic performance and seismic analysis of tied arch bridge. *Advanced Materials Research*, 446–449, 1119–1122. <https://doi.org/10.4028/www.scientific.net/AMR.446-449.1119>
- Wu, W., Wang, H., Zhu, Y., Yu, J., Zhao, H., & Zhang, H. (2018). New hanger design approach of tied-arch bridge to enhance its robustness. *KSCE Journal of Civil Engineering*, 22, 4547–4554. <https://doi.org/10.1007/s12205-018-1835-3>
- Wu, G., Ren, W. X., Zhu, Y. F., & Hussain, S. (2021). Static and dynamic evaluation of a butterfly-shaped concrete-filled steel tube arch bridge through numerical analysis and field tests. *Advances in Mechanical Engineering*, 13(9), 1–13. <https://doi.org/10.1177/16878140211044671>
- Yan, L., Li, Q. N. I., Yin, J. H., Han, C., & Cheng, M. L. (2016). Shaking table tests for Y-shaped bridges under multi-dimensional seismic excitation. *Journal of Vibration and Shock*, 35(7), 167–176. <https://doi.org/10.13465/j.cnki.jvs.2016.07.026>. (in Chinese).
- Yan, L., & Li, Q. (2017). Experimental study on Y-shaped bridge under 3-dimensional earthquake ground motions. *KSCE Journal of Civil Engineering*, 21, 2329–2337. <https://doi.org/10.1007/s12205-016-1039-7>
- Ye, Y. (2020). Urban bridgescape space construction strategy. *IOP Conference Series: Earth and Environmental Science*, 567(1), 012045. <https://doi.org/10.1088/1755-1315/567/1/012045>
- Zhang, X., Liang, N., Lu, X., Gu, A., & Shan, J. (2019). Optimization method for solving the reasonable arch axis of long-span cfst arch bridges. *Advances in Civil Engineering*, 2019, 7235656. <https://doi.org/10.1155/2019/7235656>
- Zhang, K., Qi, T., Xue, X. W., Zhu, Z., & Sun, Q. (2020). Study on the influence of cable/sling damage on the natural vibration characteristics of special-shaped cable-stayed arch bridge without back cable. *The Civil Engineering Journal*, 04, 507–517. <https://doi.org/10.14311/CEJ.2020.04.0044>
- Zhang, J. (2021). Static and dynamic characteristics and vehicle bridge coupling vibration analysis of spatial Y-shaped steel arch bridge. *Xi'an University of Architecture and Technology*. <https://doi.org/10.27393/d.cnki.gxazu.2021.000118>
- Zhou, X., & Zhang, X. (2019). Thoughts on the development of bridge technology in china. *Engineering*, 5(6), 1120–1130. <https://doi.org/10.1016/j.eng.2019.10.001>
- Zhu, Q., Cui, D., & Du, Y. (2022). Non-contact identification of bridge deflection based on network camera[J]. *Engineering Mechanics*, 39(6), 146–155. <https://doi.org/10.6052/j.issn.1000-4750.2021.03.0221>

Publisher's Note Springer Nature remains neutral with regard to jurisdictional claims in published maps and institutional affiliations.

Springer Nature or its licensor (e.g. a society or other partner) holds exclusive rights to this article under a publishing agreement with the author(s) or other rightsholder(s); author self-archiving of the accepted manuscript version of this article is solely governed by the terms of such publishing agreement and applicable law.